International Transactions on Electrical Engineering and Computer Science
Katta et.al., Vol: 2, No: 3, pp: 88-101, Sep 2023

RFMFA Technique for Islanding Detection Scheme in Integrated DG System

Katta Venkata Reddy*, Tharun Kommaddi[1]

Abstract: EEE 1547 specifies time limits for the completion of DG interconnection tasks, and one of these tasks is the detection of islanding, which must be completed within two seconds of the task's start. This thesis provides new and effective islanding detection algorithms for a hybrid distributed generating system connected to the grid. The suggested technique is a hybrid of two different optimization algorithms: Random Forest (RF) and Moth Flame Optimization (MFO). At the objective stage, this technique employs the ROCOF. The suggested methods are distinguished by their ease of use due to the lack of a mandatory minimum. Furthermore, they are unaffected by the capacity or kind of Distributed Generation linked to the utility grid and not affected by system factors. In addition, the NDZ is not present after applying these processes. When compared to the standard approaches, these methods show a marked improvement in their ability to classify events into islanding and non-islanding categories. Several elements, including varying load situations, switching operations, and network conditions, must be considered before determining the proposed solutions' viability. The MATLAB/Simulink platform provides a setting where the suggested procedures may be implemented.

Keywords: Islanding detection, Balanced islanding, RFMFA Technique, Non detection zone

1. Introduction

As existing energy sources continue to deplete at an alarming rate and environmental pollution rises, scientists have been pushed to investigate readily available renewable energy alternatives [1]. Many people are considering renewable energy options, including hydropower, tidal power, solar power, fuel cells, etc [2].

Article History
Received: 18-04-2023; Revised: 17-07-2023;
Accepted: 25-07-2023

*Corresponding author: Department of Electrical Engineering, Western New England University, Wilbraham, Springfield, MA 01119, United States

E-Mail: kv610932@wne.edu

[1] Department of Computer Science and Engineering, Technische Universitat Clausthal, Adolph-Roemer, 38678, Zellerfeld.

E-Mail: tharunkommaddi@gmail.com

Distributed generating (DG) has emerged as a major player in the electricity generating sector and the fight against global warming. Renewable energy sources (RES) are attractive because they are low-cost to maintain and easy to synchronize with the grid. Cogeneration using RES like wind and solar is prevalent in many industries to satisfy customer needs. These hybrid systems can operate autonomously or be linked to the grid [3]. The loads can be hardwired into the power system in case of an outage. Novel power electronic coherent and regulation techniques are necessary for distributed energy sources to boost effectiveness and work beyond power quality challenges. In the case of frequent fluctuations, the DG powered by a single type of renewable energy is unreliable. Combining D.G. sources in the same region might make the most efficient use of the many dispersed energy sources and guarantee a constant flow of electricity [4].

The major challenge is in securing dispersed generating units against electrical islanding and integrating them with the utility system.

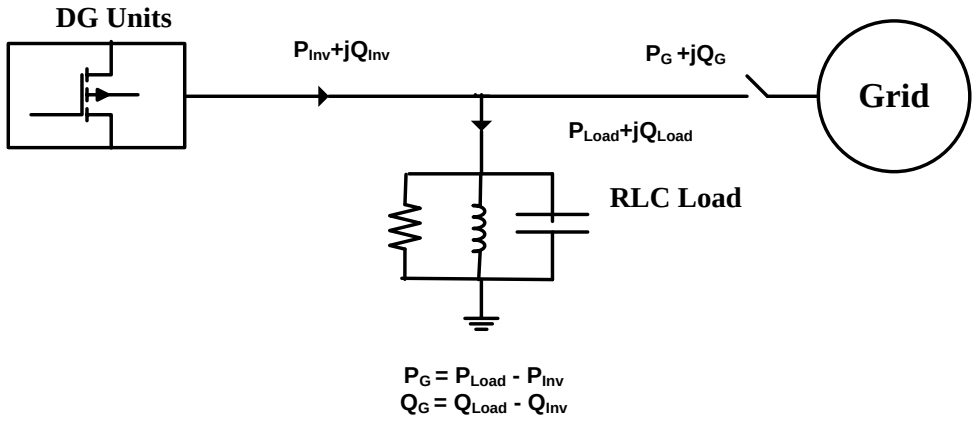

Fig. 1: D.G. source is connected to the utility grid under normal conditions.

IEEE standard 1547-2018 mandates islanding, the process by which the D.G. unit is disconnected form the electrical system throughout breaker isolation as shown in Fig.1. Islanding will lead to the occurrence of the following factors [5-8]:

- If the grid has a problem, the gadget will be turned off automatically. The unintentional activation of the usual grid supply.
- Inadvertent disconnection for maintenance at a utility point.
- In the use of grid equipment, there might be human error or deliberate troubleshooting.
- Natural disasters such as thunderstorms, hurricanes, and flooding, among others.
- When DG inverters are connected to the grid, there are several causes for islanding detection and prevention. Safety, liabilities, and retaining power quality are the most significant factors to prevent islanding. Utilities must provide their consumers with reliable electricity. As a result, anti-islanding is needed for D.G. inverters for the following reasons:
- Reclosing into an island can lead to line restriping, damage to D.G. equipment, damage to all other connecting equipment due to out-of-phase reclosing.
- The grid manual or automated restore of regular service can be affected by islanding.
- When an energized line that is thought to be disconnected from every power source remains energized due to islanding, it poses a safety risk to utility grid line employees.

In order to encourage sustainable electric power assets and increase power grid stability, it is becoming increasingly popular to connect a specific load supplied by DERs to a larger-scale electric grid so that they may share abundant electricity. Distributed power inventions often have a piece of the DER blocked to employees and equipment, which is accidentally isolated from the rest of the stage where innovation lives [9]. The "island" may be created in this scenario, and the DER can potentially maintain control over the newly established territory. Isolated DGs are a special kind of DG that gets its electricity from a source apart from the main grid. Electrical devices linked to the segment are also affected by any fluctuations in voltage or frequency in the isolated section.

2. DG system for islanding detection

When it comes to the safety of a PV system tied into the larger power grid, islanding is considered the biggest threat. Islanding in DG causes voltage and frequency instability, which hurts the solar power plant and grid [10-11]. To normalize grid-PCC functioning, these variations from the grid reference values are used during islanding mode to remove the fault. Even if the CB is unable to open the circuit, the local load will still be powered by the DG. Unexpected interference from the grid causes islanding behaviors in a PV system, as do voltage cuts, disappointed equipment, and short circuits.

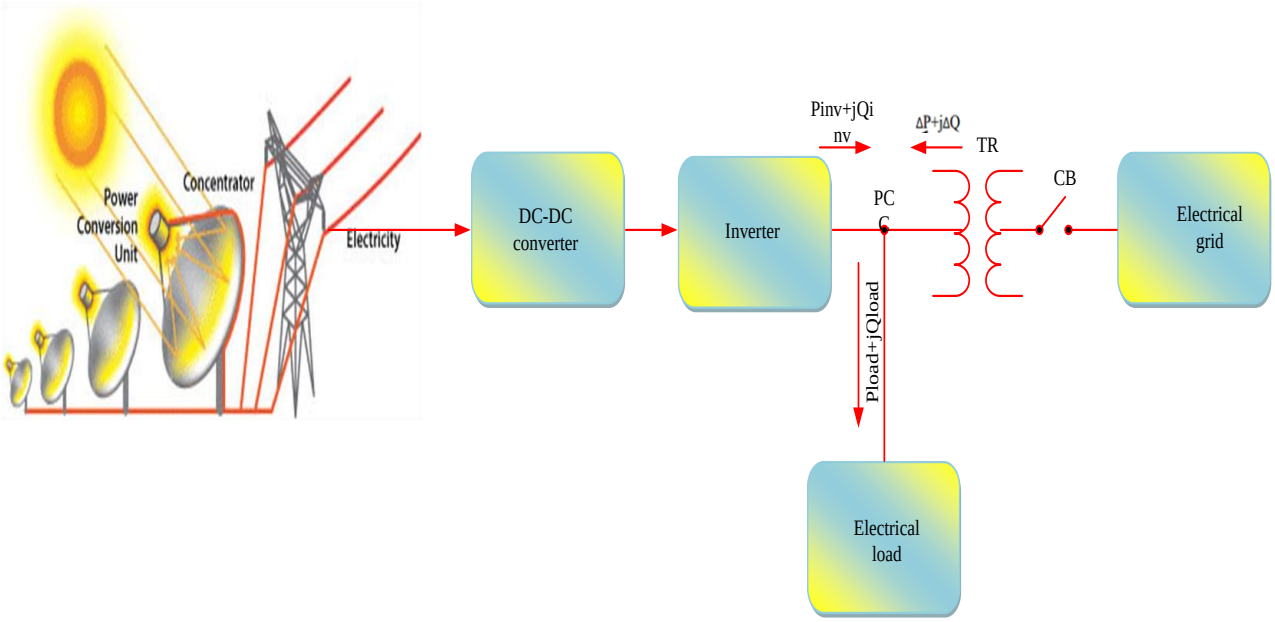

Fig.2: Using a PV-based DG system with islanding

The major components of an islanding PV-based DG system are depicted in Fig.2, shows the solar PV arrays, DC-DC boost conversion devices, and inverters for solar power with filters. Next, we'll represent these three main aspects numerically.

2.1 PV array model

A photovoltaic cell (PV) is an easy way to convert the photon energy of sunshine into usable electricity [12]. Depending on its make-up, a solar cell can produce an almost constant open circuit voltage (IPV (cell)), with the current (*I*) flowing to the associated load (*L*) being assessed in relation to the energy contained in light (photons).

$$I_{PV(cell)} = I_{ph} - I_o\left[\exp\left\{\frac{\chi\left(V_{PV}+I_{PV}R_s\right)}{\eta_k T}\right\}-1\right] - \frac{V_{PV}+I_{PV}R_s}{R_P} \quad (1)$$

Using the indexes n and m from the preceding cell equation (1), we can get the PV array equation (2) (shown below):

$$I_{PV(array)} = mI_{ph} - mI_o\left[\exp\left\{\frac{\chi\left(V_{PV(array)}+I_{PV(array)}R_s(n/m)\right)}{n\eta_k T}\right\}-1\right] - \frac{V_{PV(array)}+I_{PV(array)}R_s(n/m)}{R_p(n/m)} \quad (2)$$

The following equation (3) considers environmental factors like temperature and sunlight,

$$I_{ph} = I_{sc}\frac{I_{rrad}}{I^*_{rrad}}\left[1+\left(T-T_{ref}\right)\times k_i\right] \quad (3)$$

2.2 DC-DC converter model

The converter from DC to DC is crucial to this process since it generates the power for the DC bus [13]. The efficiency of the converter's inductance (*L*) and capacitance (*C*) may be determined with the help of the following equation.

$$L = \frac{V_i(V_o - V_i)}{\Delta I_i f_s V_o} \quad (4)$$

$$C = \frac{I_o D}{\Delta v f_s} \quad (5)$$

The following equation gives the duty cycle, *D*,

$$D = 1 - \left(\frac{V_i}{V_o} \right) \quad (6)$$

A 10% input current value and a 3% boost converter output voltage value were used in the aforementioned calculation.

2.3 PV inverter model

The two-stage PV inverters was constructed using six IGBTs. This formula [14] is used to evaluate in both a stationary and a revolving reference frame.

$$v_c = R_f I_s + L_f \frac{d(I_s)}{dt} + v_s \quad (7)$$

$$v_{cdq} = R_f I_{sdq} + L_f \frac{d(I_{sdq})}{dt} + v_{sdq} + j\omega L_f I_{sdq} \quad (8)$$

AP and RP may be determined using the following method,

$$P = \frac{3}{2} \mathrm{Re}\{v_s I_s^*\} \quad (9)$$

$$Q = \frac{3}{2} \mathrm{Im}\{v_s I_s^*\} \quad (10)$$

3. Proposed islanding detection

Information on how to create data, extract features, and find patterns is provided. Identifying and classifying IS and NIS instances in the DG system requires categorization [15]. Fig.3 is a block diagram showing how the suggested design should be implemented. When collecting data, the PCC voltage's NSC is bypassed [16]. Following analysing the processing of non-stationary signals using a sequence the analyzer, the NSV signal may be generated from the voltage signal.

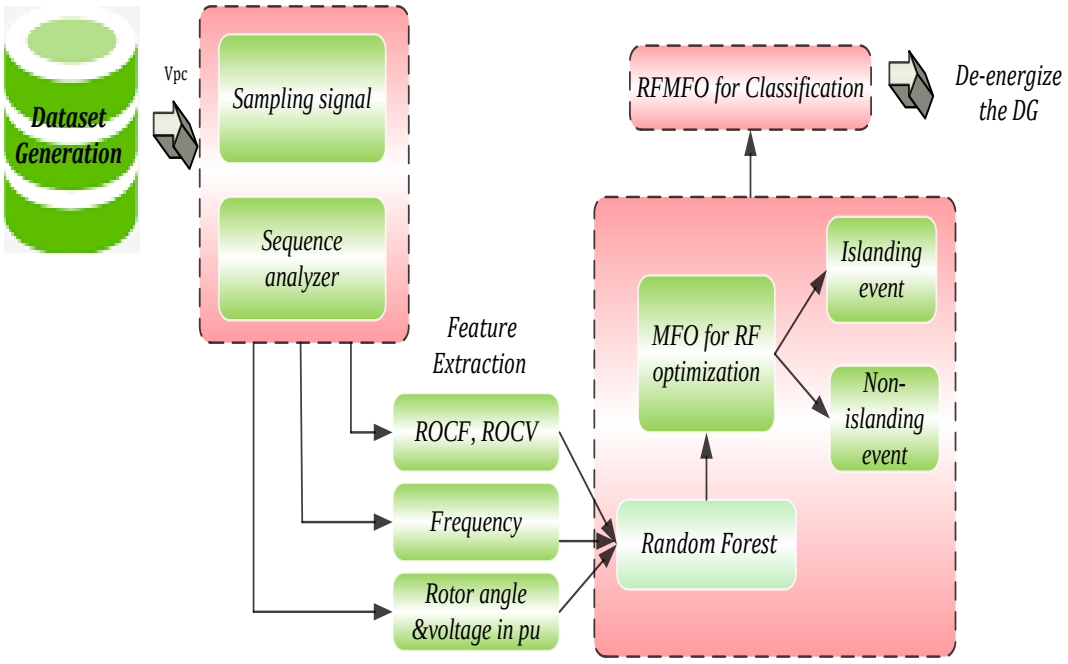

Fig. 3: Block diagram of the proposed method

In order to effectively cope with islanding detection, this work focuses on exploiting the combined RFMFO system [17-19]. The first datasets were gathered with a voltage signal in a negative sequence as the input. Five factors make up the voltage signal: frequency, frequency change rate, rotor angle, voltage in pu, and voltage change rate. Discard irrelevant data during feature extraction. Adjusted hybrid RFMFO system classifies islanding and non-islanding occurrences [20].

3.1. Data generation

The test legislation presents a wide variety of island and non-island occurrences, allowing for a rigorous scientific classification of the available data.

In an environment of islanding events, we have performed the relationship between distributed energy resources (DERs) and local load electricity consumption [21]. Both AP and RP inequality can be measured on a 0%-30% or 30%-100% scale, respectively. The tiny amount of electricity is hidden because it serves no practical purpose on the island. Non-islanding occurrences include different faults at eah bus.

3.2. Feature Extraction

When generating a set of data, feature extraction may isolate DGS problems by collecting voltage signal characteristics. System construction occurs during the islanding phase using the DG and load. A break in the utility's current injection or provision is required before the DG may begin supporting a load. Generator rotor speed is gradually raised to decrease power confusion gap [22-25]. This shifts the voltage and angle at the reference terminal. In addition, a shift in frequency is visible in the varying voltage cycle time. A standard deviation computation on a sliding data window of width T can distinguish a feature $f(t)$ from a signal $s(t)$, where t is one of the five network variables [26-27]. This technique takes data collected from the network under both IS and NIS scenarios and extracts five characteristics from those variables. The five features are mathematically expressed in Equations below, which says:

$$\sigma_v = std\{v(\tau); \quad \tau \in [t-\Delta T, t]\} \tag{11}$$

$$\sigma_f = std\{f(\tau); \quad \tau \in [t-\Delta T, t]\} \tag{12}$$

$$\sigma_\delta = std\{\delta(\tau); \quad \tau \in [t-\Delta T, t]\} \tag{13}$$

$$\sigma_{PV} = std\left\{\frac{dv(\tau)}{dt}; \quad \tau \in [t-\Delta T, t]\right\} \tag{14}$$

$$\sigma_{Pf} = std\left\{\frac{df(\tau)}{dt}; \quad \tau \in [t-\Delta T, t]\right\} \tag{15}$$

Consequently, the characteristic vectors is calculated as follows,

$$x = \left[\sigma_v \quad \sigma_f \quad \sigma_\delta \quad \sigma_{pv} \quad \sigma_{pf}\right]^T \tag{16}$$

3.3. Islanding detection using RFMFO categorization

Based on the parameters, a strong RFMFO technique is used to distinguish IS from NIS events. The suggested control approach, RFMFO, combines the benefits of RF and MFO [28]. The new RF machine learning method solves problems ensemble-style. The evolution of moths in a lunar direction provided the impetus for the development of MFOs. The technique that has been suggested places an emphasis on limiting the NDZ as much as feasible while also retaining the quality of the electricity that is generated as much as possible [29]. In this scenario, the RF is prepared for accuracy using the MFO approach, which can extract the facets inherently associated with islanding and grid disrupting effects. You will find a comprehensive example of the RF and MFO in the text that has been attached to this message.

The RF is essential to a compelling ensemble machine-learning technique that distinguishes IS and NIS events. The RF considers the overall number of trees and their average leaf count [30]. An ensemble learning approach, including the boosting and bagging procedure, is also incorporated for islanding recognition. This method uses a random selection of training samples to determine the optimal clustering. Each tree in the woods is a maximal tree because the technique uses no cutting-out procedures. Estimating the significance of variables is crucial for improving RF detection accuracy [31].

The VI is surveyed to locate the RF's input variables. Increasing detection precision with the VI is worthwhile. According to the results of the suggested method, islanding occurrences may be identified with high accuracy. The following equation describes how the training set and features are extracted for RF classification.

$$S = \{(a_1, b_1) \ , (a_2 \ , b_2) \ldots (a_n, b_n)\} \tag{17}$$

Multiple decision trees are combined to form the RF classification technique [32]. The quantity of trees in the forest is first evaluated when making a selection, and the results are listed below.

$$N = \{R_1 \ , R_2 \ , \ldots \ R_n\} \tag{18}$$

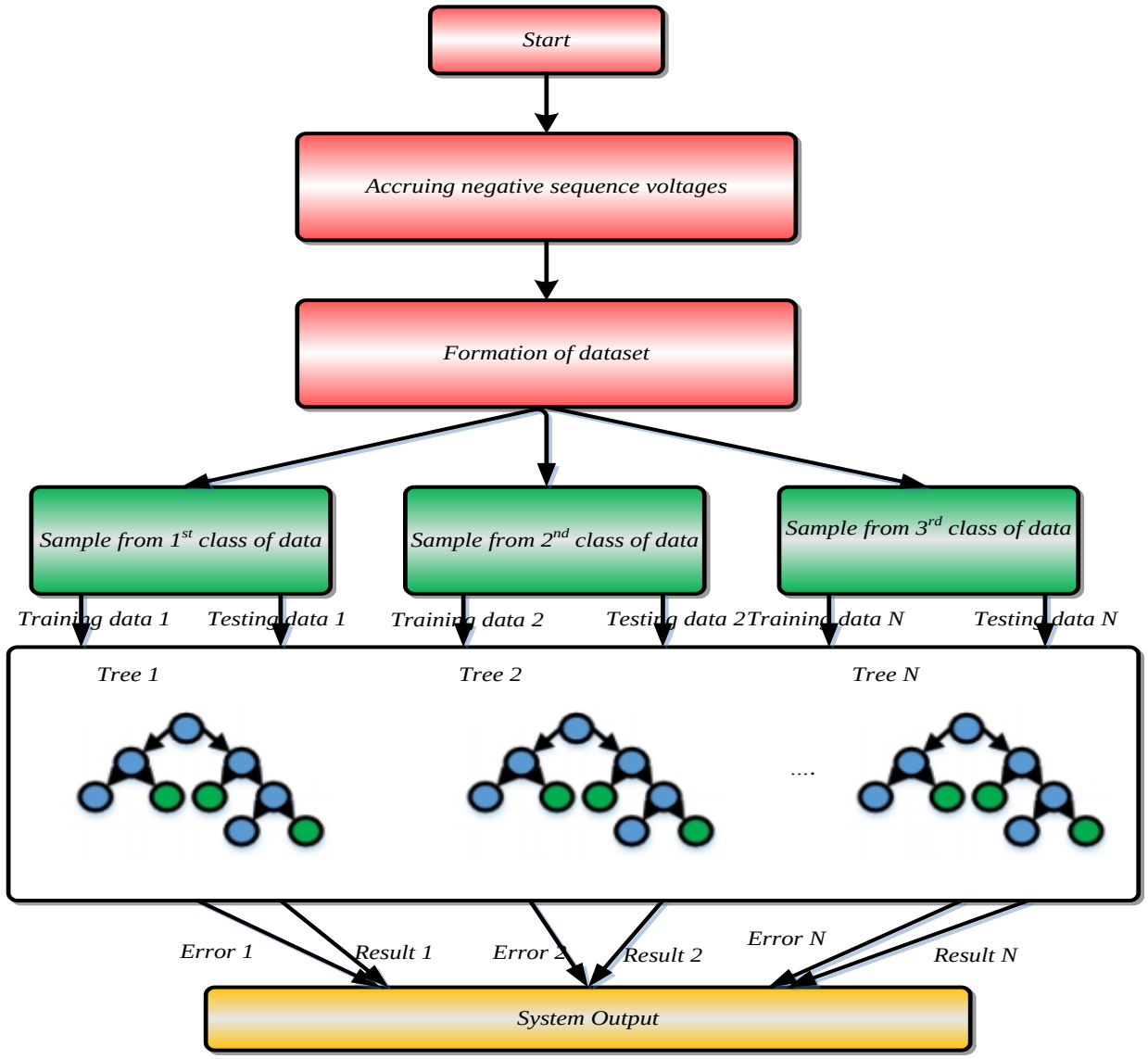

Fig. 4: Classification Process of the RF

Bootstrap samples refer to the samples taken in addition to the original sample [33-34]. Each tree is built from *S* bootstrap samples. Some input variables $D = a_1 , a_2 , \ldots a_n$ in RF classification are $b = \{b_1 , b_2 , \ldots b_n\}$. Iterated through each tree to produce output (one for each tree), as shown by. A majority vote determines the final categorization. The equation used to determine the VI is as follows:

$$V_l^{(tr)} = \frac{1}{T} \sum_{xa \in \phi^{c(tr)}} I(l_b = C_a^{tr}) - \sum_{xa \in \phi^{c(tr)}} I(l_b = C_{a,nz}^{tr}) / \phi^{c(tr)} \quad (19)$$

If the *VI* decreases under the aforementioned conditions, the accuracy grows while the precision shrinks. Different parameters were used in the tree-level execution of the suggested RF application [35]. We can model the connection between tree-level detection and the following quantities:

$$y_i = \gamma_i + \eta_i \chi_{train,ij} + \mu \quad (20)$$

In this scenario, the value is increased if the votes that were cast for the tree's segments are substantially close to the solution that should be selected. If there is no positive correlation between the segmentation replies and the real response, or if there is a negative correlation, then will be very near to zero, or even less than 0.

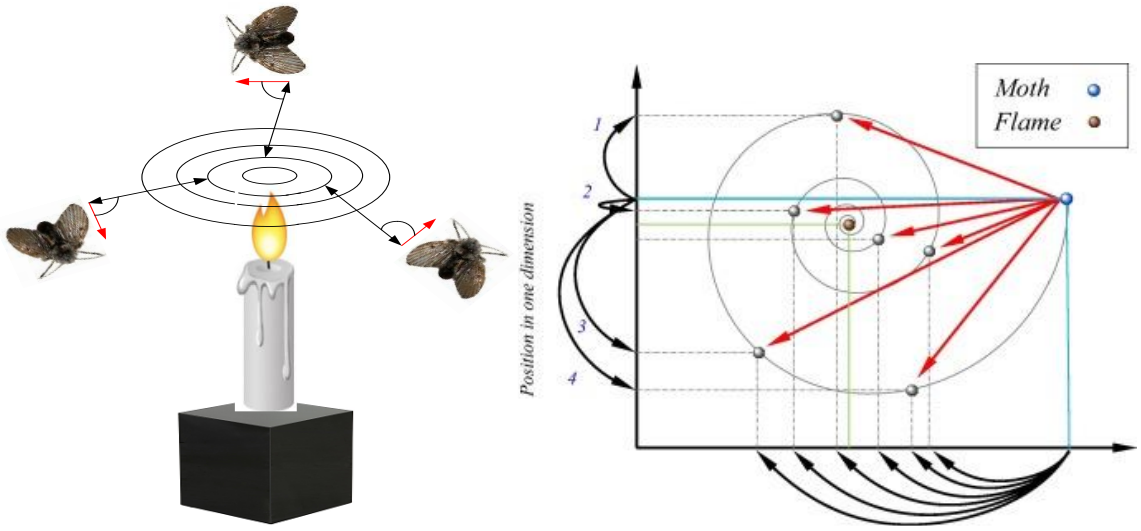

Fig. 5: a) Spiral flight towards nearby light sources b) moth logarithmic spiral position

In the overall scheme of the DG paradigm, the utility of a classifier is measured by its ability to distinguish among IS and NIS events. In the event that the value is more than some threshold, the island event has been correctly categorized. This is a sample of the RF's pseudo code, which you can get here.

Procedure for training case
Step (1): for ($i=1$) to T trees
Step (2): From the training sample, compute the bootstrap sample of size N
Step (3): By using the bootstrapped sample and the importance of the variable $V_I^{(tr)}$, the RF tree T_i is grown.
Step (4): Until reached the minimum node siz e $n_{\min}$ step 5 to 6 is repeated for each and every leaf node.
Step (5): From the variables F, some variables are randomly selected
Step (6): Among the selected variable, the best variable or split is picked.
Step (7): Output the ensemble trees $\{T_i\}_i^T$
Procedure of Testing Case
Step (8): To make a classification at a new data set x
Step (9): Compute y_i for find which class has the majority vote
$y_i = \gamma_i + \eta_i \chi_{train,ij} + \mu$

Fig. 6: Pseudo code of the RF technique

Optimisation uses the MFO technique in the recommended technique. Optimising the RF using the MFO improves tree and leaf detection in dense woods. Here, we examine the ideal number of trees and leaves per tree to distinguish between under fitting and over fitting. While under fitting is less typical, it might happen if there aren't enough trees or if each tree has a particularly small amount of leaves. The main goal of the MFO is to find the sweet spot between tree density and canopy cover. The RMSE error is used to determine the optimal tree density and leaf density. Improved performance of the RF's generated output, indicative of the island event in the DG system, is the goal of this optimisation approach. The equation detailing the split between two randomly produced trees is presented below.

$$P_{random} = random\ (d_j^d(t) - d_i^d(t) + d_i^d(t) = f_{ij}(t) \quad (21)$$

The distance calculated by Euclid between trees is,

$$S_{ij}(t) = \left\| d_i(t), c_j(t) \right\|_2 \quad (22)$$

The objective function for each particle is computed using the following equation, which accounts for false positive and negative levels.

$$X = \frac{f_{ij}(t) - worst\ (t)}{best\ (t) - worst\ (t)} \quad (23)$$

The smallest possible amount and maximisation of each and are computed as follows. The way to minimise the problem is,

$$best\ (t) = \min_{i,j\in\{1,..,N\}} fit_{ij}(t) \quad (24)$$

$$worst\ (t) = \max_{i,j\in\{1,..,N\}} fit_{ij}(t) \quad (25)$$

The maximising problem is,

$$best\ (t) = \max_{i,j\in\{1,..,N\}} fit_{ij}(t) \quad (26)$$

$$worst\ (t) = \min_{i,j\in\{1,..,N\}} fit_{ij}(t) \quad (27)$$

Finding the optimal number of leaves as well as trees

$$Y = \sum_{i,j=l_{best},\ j\neq i}^{N} rand\ \ fit_{ij}(t) \quad (28)$$

per tree is done by,

The initial specimen's fitness level has been mysteriously missing. The optimal forest tree, with leaves on each tree, is provided by the MFO.

4. Results and Discussions

We discuss the three major steps of the proposed RFMFO technique: data production, feature extraction, and IS and NIS DG event detection. The suggested RFMFO method's simulation outcomes are contrasted with those of well-established methods including the Artificial Neural Network, the SVM, the Decision Tree, and the Naive Bayesian classifier. The proposed method is evaluated during a voltage dip, a voltage rise, a voltage sag, and a voltage swell. Using the MATLAB/Simulink environment, we examine how well the proposed method works in practise. The following diagrams outline the specifics the test cases.

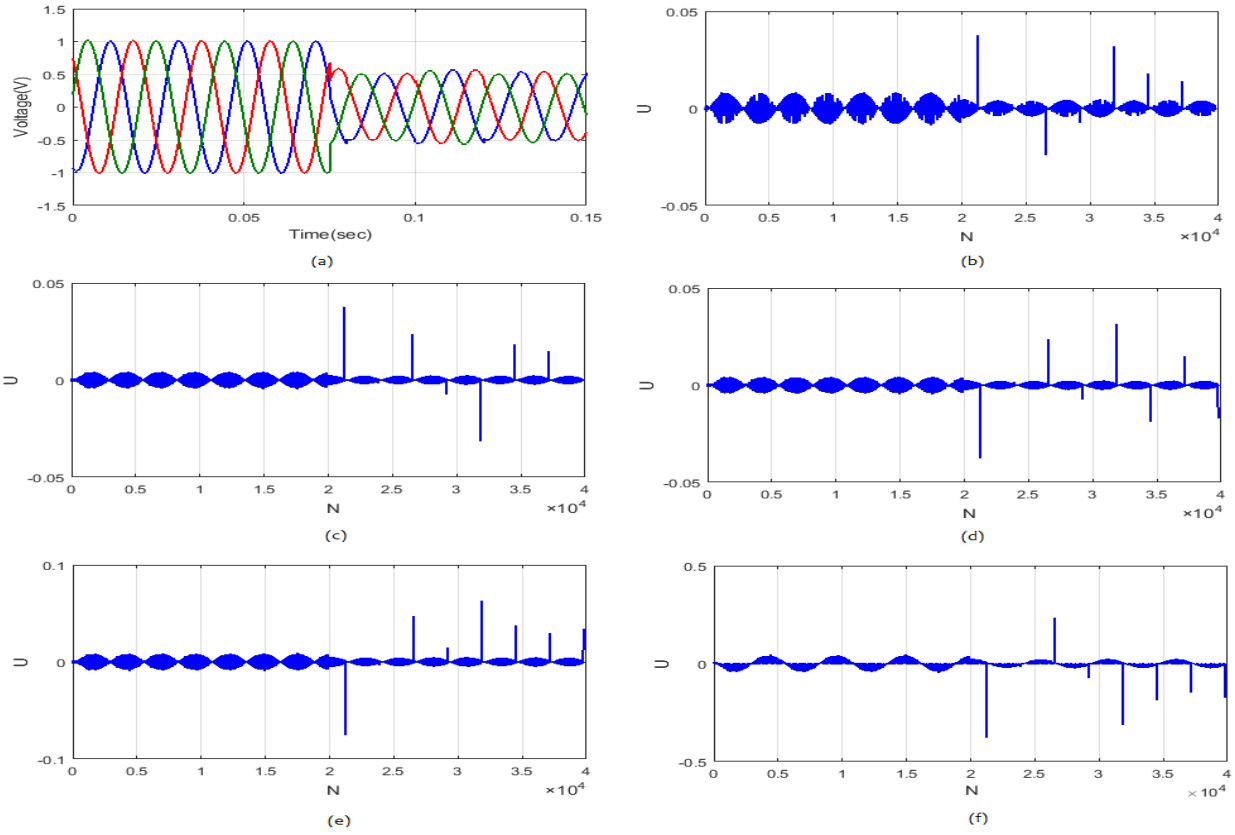

Fig. 7: Islanding voltage loss at the PCC for varying transform coefficient sizes (a) 3- ϕ voltage (b) Scale 1 (c) Scale 2 (d) Scale 3 (e) Scale 4 (f) Scale 5 .

The PCC in Fig.7 for a range of transform coefficient values. Subplot 7(a) in Fig.7 shows the three-phase voltage of DG produced between 0 and 0.15 seconds. The 3- ϕ voltage is shown to be uniform and one during the first 0.075 seconds of the plot, before dropping to a minimum of 0.5 V and staying there until the end of system operation. Voltage decrease from scale 1 to scale 5 is shown in subplot 7(b)–(f). The total number of data points used to create these graphs is 4104. Voltage decreases from 2104 to 4104 N are seen in Graphs 7(b)–(f). Fig.8 depicts how adjusting the magnitude of the transform coefficients affects the peak voltage during islanding at PCC. Fig.8, subplot 7(a), shows the 3- ϕ voltage of DG. This graph shows that during the first 0.075 seconds of system operation, the 3- ϕ voltage is balanced and unity but may become unbalanced and not unity for the remainder of the period. Voltage increases from scale 1 to scale 5 are shown in subplot 7(b)–(f). A rise in PCC voltage between 2.1 104 and 4 104 N is shown in figures 6(b)–(f). Figure 8 depicts the voltage drop brought on by the disturbances at various scales. Fig.8(a) is a subplot of Fig.8 showing the 3- ϕ voltage of DG. During the first 0–0.05 seconds of this graph, the voltage is uniform and stable at unity. The voltage then drops between 0.005 and 0.1 seconds as a result of voltage fluctuations, before returning to unity and being stable for the remainder of the procedure. Subplots 9(b)–9(f) show a drop in voltage between 1.4104 N and 2.7104 N. Fig.9 depicts the voltage surge induced by the disturbances at various scales. Fig.10(a) is a subplot of the full figure depicting the three-phase voltage of DG. Between 0.005 and 0.1 seconds, the voltage on this graph is constant and even at unity. Voltage surged because to disturbances in the remaining time frame. The voltage increase is shown in subplots Fig.10(b)–(f), which span the range from 0 to 1.4 104 N and 2.7 104 – 4 104 N, respectively. Fig.8 depicts how adjusting the magnitude of the transform coefficients affects the peak voltage during islanding at PCC. Fig.8, subplot 8(a), shows the 3- ϕ voltage of DG. This graph shows that during the first 0.075 seconds of system operation, the 3- ϕ voltage is balanced and unity but may become unbalanced and not unity for the remainder of the period.

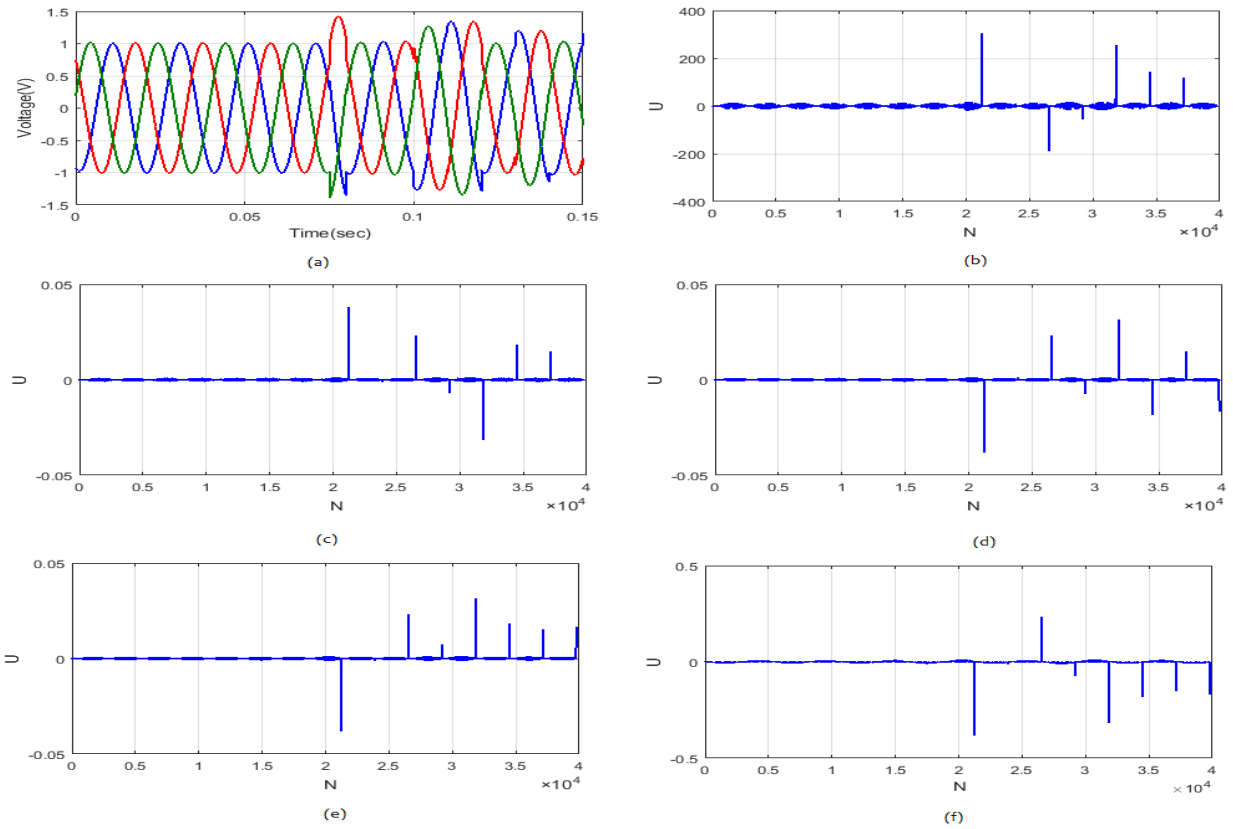

Fig. 8: Islanding voltage increases at the PCC for a range of transform coefficient sizes. (a) 3- ϕ voltage (b) Scale 1 (c) Scale 2 (d) Scale 3 (e) Scale 4 (f) Scale 5

4.1. Performance Analysis

Table.1 below summarises the results of the RFMFO algorithm's testing. Three types of mistakes are examined to determine how well the proposed RFMFO method performs. The absolute size of the root-mean-squared error (RMSE) must be rather large if the detection results are so distant from the target values. A negative MBE value indicates an underestimation of the detection, while a positive value indicates an overestimation. MAPE is a reliable indicator of precision. It is common practise to convey RMSE, MBE, and MAPE as targets,

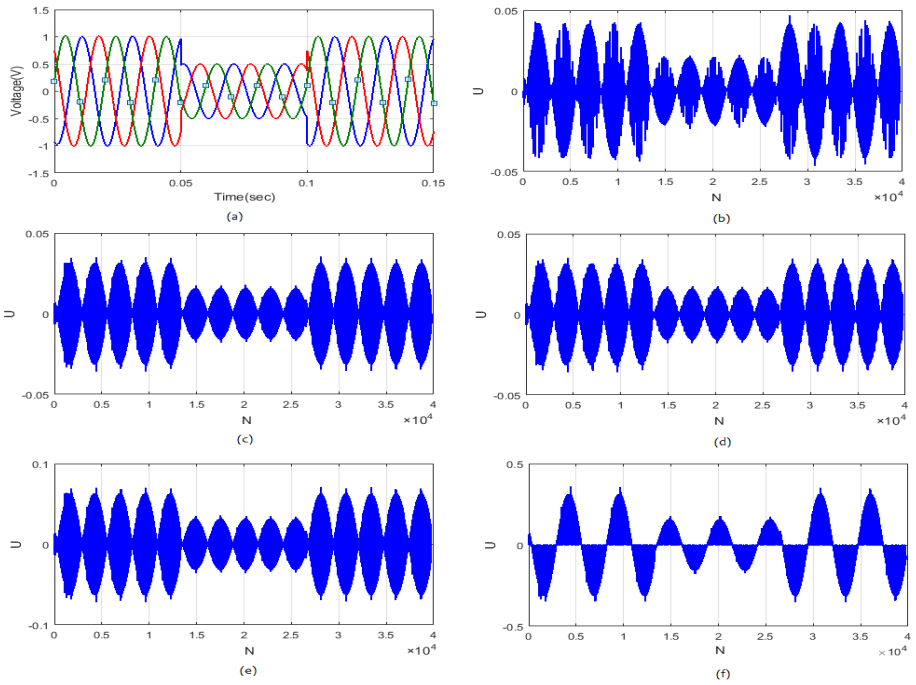

Fig. 9: Disturbance-induced voltage dips at various transform coefficient scales (a) 3- ϕ voltage (b) Scale 1 (c) Scale 2 (d) Scale 3 (e) Scale 4 (f) Scale 5

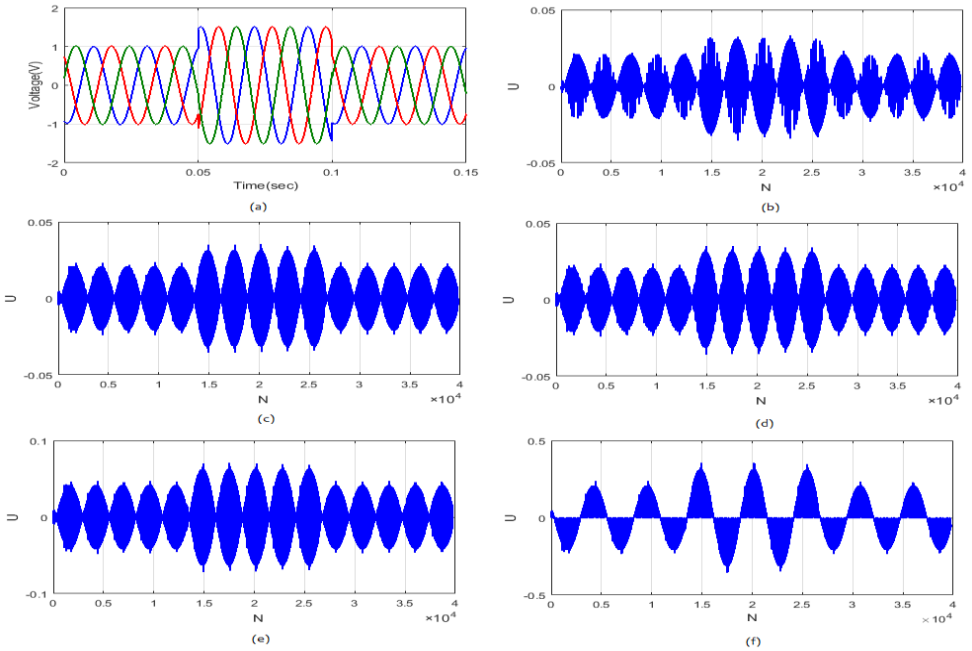

Fig. 10: Disturbance-induced voltage rise at various scales of transform coefficients (a). 3- ϕ voltage (b) Scale 1 (c) Scale 2 (d) Scale 3 (e) Scale 4 (f) Scale 5

$$RMSE = \sqrt{\frac{1}{z}\sum_{m=1}^{z}(I_m - I_{pm})} \quad (29)$$

$$MAPE = \frac{1}{z}\sum_{m=1}^{z}\left|\frac{I_m - I_{pm}}{I_m}\right| a \quad (30)$$

$$MBE = \frac{1}{z}\sum_{m=1}^{z} I_{pm} - I_m \quad (31)$$

The goal value, projected value, and number of

Table.1: RFMFO Detection outcomes

Samples	Voltages at PCC	Number of samples	Number of misclassifications	Classification rate (%)
Islanding	Voltage Rises	120	3	98.5
	Voltage Drops	120	1	98.65
Disturbances	Voltage Swells	120	2	99.43
	Voltage sags	120	1	97.65

Table.1 provides a statistical breakdown of the proposed approach. This research compares the suggested RFMFO islanding detection approach against state-of-the-art classification methods to determine its efficacy. The proposed method finishes 50 attempts in 1 minute and 99 milliseconds with a mean bias error (MBE) of 1.23 and a root-mean-squared error (RMSE) of 7.63.

Table.2: The suggested method is compared to the current one statistically for 50 and 100 trials of islanding.

Metrics	Naïve Bayesian	SVM	DT	RF	ANN	Proposed
	50 trails					
RMSE	26.43	18.91	23.43	10.65	8.52	7.63
MAPE	17.23	6.76	13.54	1	0.99	0.93
MBE	7.56	2.68	5.73	2.87	1.78	1.23
Consumption time (s)	7.67	6.67	8.67	5.54	2.96	1.99
	100 trails					
RMSE	29.78	21.57	26.78	13.67	9.36	8.65
MAPE	18.55	7.78	14.67	2.56	1	0.67
MBE	10	5.58	8.89	5.75	3.87	2.69
Consumption time (s)	8.77	7.44	8.37	6	2.98	1.58

After applying the suggested technique to a total of 100 trials, the average RMSE, MAPE, and MBE were 8.65%, 0.675%, respectively. Table. 2 shows the recommended method's statistical analysis. This work compares the suggested RFMFO islanding detection approach to various well-established classification methods. The recommended method completes 50 trials in 1.99 seconds with 7.63, 0.93, and 1.23 RMSE, MAPE, and MBE. After 100 trials, the suggested technique reduces RMSE, MAPE, and MBE to 8.65%, 0.67 percent, and 2.69 seconds, respectively. True negative (TN) rates are used to determine the level of specificity. Both the positive and negative rates are used in the calculation of accuracy. The following formulas can be used to calculate the recall, specificity, accuracy, and precision.

$$Specifi\ city = \frac{TN}{TN + FP} \quad (32)$$

$$Accuracy = \frac{TP + TN}{TP + TN + FP + FN} \quad (33)$$

$$\Pr ecision = \frac{TP}{TP + FP} \quad (34)$$

$$recall = \frac{TP}{TP + FN} \quad (35)$$

Sum of the true positives (TP), false negatives (FN), missing samples (FP), and samples misidentified as noise lesions (TN).

Table.3: Inter-turn insulation fault performance evaluation using proposed and existing methods for 50 and 100 trials

Performance measures	Naïve Bayesian	SVM	DT	RF	ANN	Proposed
	50 trails					
Accuracy	0.55	0.75	0.85	0.90	0.91	1.23
Specificity	0.5	0.7	0.8	0.9	0.94	1.54
Recall	0.6	0.8	0.9	1	1.53	1.98
Precision	0.52	0.72	0.82	0.9	0.96	1.54
	100 trails					
Accuracy	0.6	0.7	0.8	0.9	0.93	1.43
Specificity	0.53	0.63	0.75	0.85	0.9	0.95
Recall	0.57	0.6	0.85	0.8	0.85	0.92
Precision	0.55	0.65	0.72	0.95	0.98	1.43

Table.3 compares the two approaches across 50 and 100 attempts of islanding defects for reliability, specificity, recollection, and precise. In 50 trials, the suggested method had an accuracy of 1.23%, a

specificity of 1.54%, a recall of 1.98%, and a precision of 1.54%. There is a 0.55% margin of error, a 0.50% specificity margin, a 0.60% recall margin, and a 0.52% accuracy margin using the currently used method. SVM use periods of 0.75, 0.7, 0.8, and 0.72. Accuracy, specificity, recall, and precision for DT fall between 0.85 to 0.90. Confidence intervals of 0.90 are achieved for all four metrics (accuracy, specificity, recall, and precision) when RF is used for measurement. The accuracy, specificity, recall, and precision of ANN can be anywhere from 0.91 to 0.96. With 100 iterations, the recall of the proposed approach is 0.92 and the accuracy is 1.43. It has a reliability of 1.43. The aforementioned current technique has an accuracy, specificity, recall, and precision of between 0.6% and 0.57 when employing a naïve Bayesian analysis. SVM allows for values between 0.7 and 0.63, as well as between 0.6 and 0.65. Accuracy, specificity, recall, and precision can fall anywhere between 0.80 to 0.85 in DT. Accuracy, specificity, recall, and precision can be anywhere between 0.90 and 0.95 in RF. Accuracy, specificity, recall, and precision can range from 0.93 to 0.98 in ANN. The proposed method significantly outperforms the aforementioned conventional approach in terms of precision and accuracy.

5. Conclusion

Taking into account the unique characteristics of NSV signals, this dissertation introduces the hybrid RFMFO approach for islanding detection. In the DG structure of PV generating circuits attached to low-voltage lines, the PCC voltage is used to extract characteristics from the NSV signal to identify IS and NIS occurrences. There is no additional expense, no negative impact on electricity quality, and no power consumption from using the suggested approach for establishing the island's condition. The findings can identify island occurrences even in the simplest case, where the intrinsic power generated is directly correlated to the localised load utilisation. Using the procedure, the NDZ may be eradicated. Simulation findings demonstrate that the suggested approach successfully isolates islanding from all other events. Furthermore, this technique can avoid the issue of permanently establishing location thresholds, which is a concern with the present alternatives.

Conflict of Interest

The authors declare “No conflict of interest”

References

[1] M. Mishra, and P. K. Rout “Fast discrete s-transform and extreme learning machine based approach to islanding detection in grid-connected distributed generation”, *Energy Systems*, Vol. 10, No. 3, pp. 757-789, 2019.

[2] O. P. Mahela, Y. Sharma, S. Ali, B. Khan and A. R. Garg “Voltage-based hybrid algorithm using parameter variations and Stockwell transform for islanding detection in utility grids”, *In Informatics*, Vol. 8, No. 2, art.no. 21, 2021.

[3] S. Cheol, P. K. Ray, and S. R. Salkuti “Islanding detection in a distribution network with distributed generators using signal processing techniques”, *International Journal of Power Electronics and Drive Systems*, Vol. 11, No. 4, pp. 2099-2106, 2020.

[4] M. Padhee, P. K. Dash, K. R. Krishnanand and P. K. Rout “A fast Gauss-Newton algorithm for islanding detection in distributed generation”, *IEEE Transactions on Smart Grid*, Vol. 3, No. 3, pp. 1181-1191, 2012.

[5] V. L. Merlin, R. C. D. Santos, A. P. Grilo, J. C. M. Vieira, D. V. Coury and M. Oleskovicz “A new artificial neural network based method for islanding detection of distributed generators”, *International Journal of Electrical Power & Energy Systems*, Vol. 75, pp. 139-151, 2016.

[6] H. Samet, F. Hashemi and T. Ghanbari “Minimum non detection zone for islanding detection using an optimal Artificial Neural Network algorithm based on PSO”, *Renewable and Sustainable Energy Reviews*, Vol. 52, pp. 1-18, 2015.

[7] S. Admasie, S. B. A. Bukhari, T. Gush, R. Haider, and Ch. Kim, “Intelligent islanding detection of multi-distributed generation using artificial neural network based on intrinsic mode function feature. *Journal of Modern Power Systems and Clean Energy*, Vol. 8, No. 3, pp. 511-520, 2020.

[8] F. Hashemi, M. Mohammadi and A. Kargarian “Islanding detection method for microgrid based on extracted features from differential transient rate of change of frequency”, *IET*

Generation, Transmission and Distribution, Vol. 11, No. 4, pp. 891-904, 2017.

[9] W. Ali, A. Ulasyar, M. U. Mehmood, A. Khattak, K. Imran, H. S. Zad, and S. Nisar "Hierarchical control of microgrid using IoT and machine learning based islanding detection", *IEEE Access*, Vol. 9, pp. 103019-103031, 2021.

[10] B. Matic-Cuka and M. Kezunovic "Islanding detection for inverter-based distributed generation using support vector machine method" *IEEE Transactions on Smart Grid*, Vol. 5, No. 6, pp. 2676-2686, 2014.

[11] P. K. Dash, S. K. Barik, and R. K. Patnaik "Detection and classification of islanding and nonislanding events in distributed generation based on fuzzy decision tree", *Journal of Control, Automation and Electrical Systems*, Vol. 25, No. 6, pp. 699-719, 2014.

[12] B. Zhou, C. Cao, C. Li, Y. Cao, C. Chen, Y. Li and L. Zeng "Hybrid islanding detection method based on decision tree and positive feedback for distributed generations", *IET Generation, Transmission & Distribution*, Vol. 9, No. 14, pp. 1819-1825, 2015.

[13] S. R. Samantaray, K. El-Arroudi, G. Joos and I. Kamwa "A fuzzy rule-based approach for islanding detection in distributed generation", *IEEE transactions on power delivery*, Vol. 25, No. 3, pp. 1427-1433, 2010.

[14] S. S. Madani, A. Abbaspour, M. Beiraghi, P. Z. Dehkordi and A. M. Ranjbar "Islanding detection for PV and DFIG using decision tree and AdaBoost algorithm", *In 2012 3rd IEEE PES Innovative Smart Grid Technologies Europe*, pp. 1-8, 2012.

[15] E. C. Pedrino, T. Yamada, T. R. Lunardi and J. C. M. Vieira "Islanding detection of distributed generation by using multi-gene genetic programming based classifier", *Applied Soft Computing*, Vol. 74, pp. 206-215, 2019.

[16] W. J. Chiang, H. L. Jou, J. C. Wu, K. D. Wu and Y. T. Feng "Active islanding detection method for the grid-connected photovoltaic generation system", *Electric Power Systems Research*, Vol. 80, No. 4, pp. 372-379, 2010.

[17] C. L. Trujillo, D. Velasco, E. Figueres and G. Garcerá "Analysis of active islanding detection methods for grid-connected micro inverters for renewable energy processing", *Applied Energy*, Vol. 87, No. 11, pp. 3591-3605, 2010.

[18] Y. Li, S. Li, S. Bai and C. Niu "Frequency-feedback based islanding detection algorithm for micro-grid", *Transactions of Tianjin University*, Vol. 14, No. 2, pp. 85-91, 2008.

[19] H. H. Zeineldin and S. Kennedy "Sandia frequency-shift parameter selection to eliminate nondetection zones", *IEEE Transactions on Power Delivery*, Vol. 24, No. 1, pp. 486-487, 2008.

[20] M. V. Reis, T. A. Barros, A. B. Moreira, E. Ruppert and M. G. Villalva "Analysis of the Sandia Frequency Shift (SFS) islanding detection method with a single-phase photovoltaic distributed generation system", *In 2015 IEEE PES Innovative Smart Grid Technologies Latin America*, 125-129, 2015.

[21] L. A. Lopes and H. Sun "Performance assessment of active frequency drifting islanding detection methods", *IEEE Transactions on Energy Conversion*, Vol. 21, No. 1, pp. 171-180, 2006.

[22] B. Wen, D. Boroyevich, R. Burgos, Z. Shen and P. Mattavelli "Impedance-based analysis of active frequency drift islanding detection for grid-tied inverter system", *IEEE Transactions on industry applications*, Vol. 52, No. 1, pp. 332-341, 2015.

[23] G. K. Hung, C. C. Chang and C. L. Chen "Automatic phase-shift method for islanding detection of grid-connected photovoltaic inverters", *IEEE Transactions on energy conversion*, Vol. 18, No. 1, pp. 169-173, 2003.

[24] F. Liu, Y. Kang, Y. Zhang, S. Duan and X. Lin "Improved SMS islanding detection method for grid-connected converters", *IET renewable power generation*, Vo. 4, No. 1, pp. 36-42, 2010.

[25] S. Dutta, P. K. Sadhu, M. J. B. Reddy and D. Mohanta "Shifting of research trends in islanding detection method-a comprehensive survey", *Protection and Control of Modern Power Systems*, Vol. 3, No. 1, pp. 1-20, 2018.

[26] M. V. Reis, M. G. Villalva, T. A. Barros, A. B. Moreira and E. Ruppert "Active frequency drift with positive feedback anti-islanding method for a single phase two-stage grid-tied photovoltaic system", *In 2015 IEEE 13th Brazilian Power Electronics Conference and 1st Southern Power Electronics Conference,* 1-6, 2015.

[27] R. Azim, F. Li, Y. Xue, M. Starke, and H. Wang "An islanding detection methodology combining decision trees and Sandia frequency shift for inverter-based distributed generations", *IET Generation, Transmission & Distribution*, Vol. 11, No. 16, pp. 4104-4113, 2017.

[28] A. Y. Hatata, E. H. Abd-Raboh and B. E. Sedhom "Proposed Sandia frequency shift for anti-islanding detection method based on artificial immune system", *Alexandria engineering journal*, Vol. 57, No. 1, pp. 235-245, 2018.

[29] M. Pahlevani, S. M. Kaviri, P. Jain and B. Mohammadpour "Advanced slip mode frequency shift islanding detection method for single phase grid connected PV inverters", *In 2016 IEEE Applied Power Electronics Conference and Exposition*, pp. 378-385, 2016.

[30] Y. Gao and J. Ye "Improved slip mode frequency-shift islanding detection method", *In 2019 International Conference on Virtual Reality and Intelligent Systems*, pp. 152-155, 2019.

[31] B. K. Panigrahi, A. Bhuyan, J. Shukla, P. K. Ray, and S. Pati "A comprehensive review on intelligent islanding detection techniques for renewable energy integrated power system", *International Journal of Energy Research*, Vol. 45, No. 10, pp. 14085-14116, 2021.

[32] N. Shafique, S. Raza, S. Bibi, M. Farhan and M. Riaz "A simplified passive islanding detection technique based on susceptible power indice with zero NDZ", *Ain Shams Engineering Journal*, Vol. 13, No. 4, art.no. 101637, 2022.

[33] S. Kumar, M. Kumar and J. Kumar "Change in Negative Sequence Current-Based Islanding Event Detection", *In Recent Advances in Power Systems*, pp. 39-49, 2022.

[34] V. Bindu and T. Anuradha. "Review of islanding detection using advanced signal processing techniques", *Electrical Engineering*, pp. 1-22, 2023.

[35] T. Funabashi, K. Koyanagi, and R. Yokoyama "A review of islanding detection methods for distributed resources", *In 2003 IEEE Bologna Power Tech Conference Proceedings*, Vol. 2, pp. 6-15, 2003.

[36] O. Raipala, A. Mäkinen, S. Repo and P. Järventausta "An anti-islanding protection method based on reactive power injection and ROCOF", *IEEE Transactions on power delivery*, Vol. 32, No. 1, pp. 401-410, 2016.

[37] S. Murugesan, V. Murali and S. A. Daniel "Hybrid analyzing technique for active islanding detection based on d-axis current injection", *IEEE Systems Journal*, Vol. 12, No. 4, pp. 3608-3617, 2017.

[38] A. Emadi and H. Afrakhte "A reference current perturbation method for islanding detection of a multi-inverter system", *Electric Power Systems Research*, Vol. 132, pp. 47-55, 2016.

[39] A. Kumar, P. K. Panda, A. Mohapatra, S. N. Singh and S. C. Srivastava "Mode of oscillation based islanding detection of inverter interfaced DG using ESPRIT", *Electric Power Systems Research*, Vol. 200, art.no. 107479, 2021.

***